Available online at www.sciencedirect.com
SCIENCE DIRECT®
ELSEVIER
European Journal of Mechanics B/Fluids 22 (2003) 239–258

Hydrodynamic stability of the Ekman boundary layer including interaction with a compliant surface: a numerical framework

Leanne Allen, Thomas J. Bridges

Department of Mathematics and Statistics, University of Surrey, Guildford, Surrey GU2 7XH, UK

Received 19 September 2002; received in revised form 15 April 2003; accepted 20 April 2003

Abstract

A model is developed for the interaction of the Ekman boundary layer with a compliant two-dimensional surface. To study the hydrodynamic instability of this interaction a new accurate numerical framework extending the compound matrix method is introduced. Preliminary results are presented on the implications of the compliant surface on the stability of the Ekman layer which show that the compliant surface has negligible effect on the critical Reynolds number.

1. Introduction

The Ekman boundary layer is an exact solution of the three-dimensional Navier–Stokes equations, and it is fundamental to the theory of ocean circulation. In an infinite ocean on a non-rotating Earth, the seawater would always move in the same direction as the wind that set it in motion. On a rotating Earth, the surface water is deflected to the right (left) of the wind in the northern (southern) hemisphere. Historically, the oceanographer Nansen observed that the drift of surface ice was angled at 20–40 degrees to the right of the wind direction in the northern hemisphere, and he attributed this effect to the Coriolis force. Although the rotation rate is small, the Coriolis force is not negligible compared to the slow drift velocities. Based on this suggestion, in 1905 the Swedish physicist Ekman [1] studied the equations of motion showing that a balance between the pressure gradient, the Coriolis force and frictional term resulted in an exact solution, in the absence of horizontal boundaries. The Ekman solution shows that motion of each deeper layer is deflected to the right of the one above. The mean velocity can be represented by a vector that decreases in magnitude exponentially with depth and changes angle linearly with depth forming a spiral when viewed from above, now called the *Ekman spiral*, as shown in Fig. 1. Ekman spiral flows can be created in the laboratory and have been observed in both atmospheric and oceanic flows. For example, boundary layer velocity profiles that approximate the Ekman layer occur in the atmospheric boundary layer to a height of about 1000 m, and in wind driven surface layers of the ocean to a depth of the order of 50 m [2]. Although oceanic and atmospheric examples of Ekman layers always involve turbulence, due to the rough boundary surfaces, one can assume that the mean flow is steady and laminar.

The steady laminar Ekman layer is an exact solution of the Navier–Stokes equations, making it attractive for theoretical analysis. It has the added advantage that it is a boundary layer with a constant geostrophic velocity and constant boundary layer thickness, and so it is strictly parallel. In this paper the interaction of the Ekman layer with a compliant surface is modelled and analyzed. As far as we are aware, this interaction has never been studied, and as far as we are aware there is no obvious application of this interaction. The motivation in this paper is fundamental: to consider the Ekman layer as a prototype of a three-dimensional rotating flow, and to use it to get insight into the effect of an adjacent compliant surface on the hydrodynamic stability of rotating three-dimensional flows. For two-dimensional boundary layers, there is already substantial evidence for transition delay due to the boundary layer flow interacting with a compliant surface (Carpenter [3]).

E-mail address: t.bridges@surrey.ac.uk (T.J. Bridges).

0997-7546/03/$ – see front matter
doi:10.1016/S0997-7546(03)00036-0

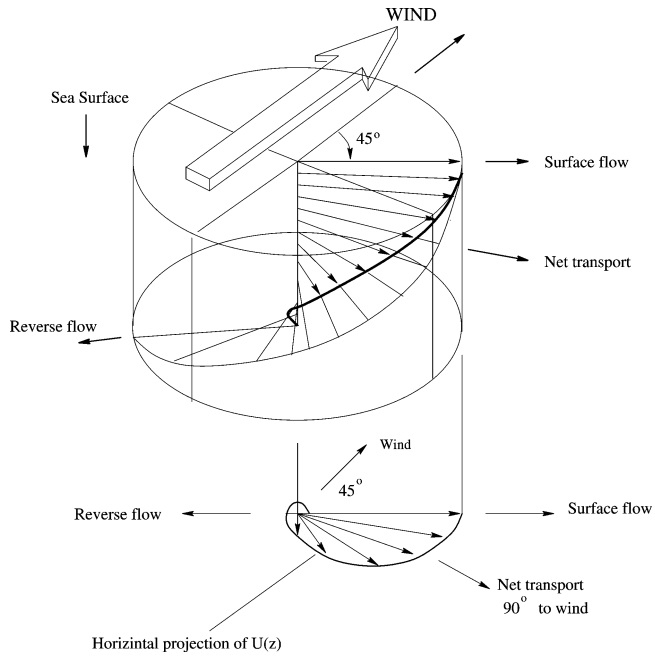

Fig. 1. A schematic of the Ekman spiral illustrating geostrophic oceanic flow induced by wind stress in the northern hemisphere. (Diagram reproduced from Vanyo [2].)

The hydrodynamic stability of the Ekman layer adjacent to a rigid surface has been thoroughly researched, starting with the work of Lilly [4], e.g., [5–14]. Theory has confirmed the existence of two forms of instability in the Ekman layer. These are referred to as *type*-1 and *type*-2 instabilities. The type-1 instability is an inviscid cross-flow type instability and is a consequence of an inflection point in the velocity profile, whereas the type-2 instability is a travelling wave of viscous type, similar to a Tollmien–Schlichting mode.

The experiment of Faller [15] was concerned with the stability of the steady laminar boundary-layer flow of a homogeneous fluid which occurs in a rotating system when the relative flow is slow compared to the basic speed of rotation. Ekman flow was produced in a large cylindrical rotating tank by withdrawing water from the centre and introducing it at the rim. This created a steady-state symmetrical vortex in which the flow from the rim to the centre took place entirely in the shallow viscous boundary-layer at the bottom. In these experiments, an unstable boundary layer was detected above a critical Reynolds number of about 125, now known to be the type-1 instability. However, Faller and Kaylor [16] obtained numerical solutions to the time dependent non-linear equations of motion starting with a perturbation on the finite difference equivalent of a laminar Ekman solution, and the numerics showed the presence of the two distinct modes of instability.

At about the same time, the theory of Lilly [4] confirmed the existence of the type-1 instability, but he also found that the most unstable mode for the Ekman layer is a travelling type-2 mode with a critical Reynolds number of around 55 and angle of orientation relative to the x-axis (i.e., the direction of the primary pressure gradient) approximately $\varepsilon = -20$ degrees. The most accurate values to date for the critical Reynolds number are due to Melander [6] who found $R_e \approx 54.155042$ with $\varepsilon \approx -23.3261°$. The onset of the type-1 stationary wave instability is predicted theoretically to occur at a Reynolds number of about 112.75.

Although type-2 travelling waves have a significantly lower critical Reynolds numbers than the type-1 waves, it is the latter that are more commonly observed in experiments. Analysis of the relative growth rates of the two modes reveals a more rapid growth associated with the inviscid type-1 mode, which would suggest that even though it is the viscous type-2 mode which first becomes unstable, the growth of the inviscid mode would be sufficiently greater than the former to dominate at higher Reynolds numbers. This provides an explanation for the difficulty in detecting the type-2 mode at higher Reynolds numbers in experiments. However, it could also be due to experimental measurement techniques that filter out travelling waves; see §5 of [4] for a discussion of this point. Indeed Faller [15] did in fact detect the type-2 instability and noted qualitative features essentially corresponding to Lilly's numerical results, although, it was observed erratically.

The laminar Ekman layer has similarities with the Von Karman boundary layer (steady axisymmetric incompressible flow due to an infinite disk rotating in a still fluid). Whilst studying the stability of the Von Karman boundary layer, Lingwood [17] discovered the significance of a third class of instabilities, which was first noticed by Mack in 1985 [18]. This third class is

an absolute instability produced by a coalescence of the inviscidly-unstable mode and a third mode that is spatially damped and inwardly propagating. Although, it is difficult to confirm the existence of an absolute instability experimentally, because absolute instability is a theoretical concept based on spatially homogeneous systems and an experiment would examine the global response of the real spatially inhomogeneous flow, experiments of Lingwoood provided strong evidence for the physical significance of this absolute instability. Direct numerical simulations of Davies and Carpenter [19,20] of the real, spatially inhomogeneous, flow showed that there is no linear amplified global mode associated with the absolute instability in the case of the rotating-disc boundary layer, and this is fully consistent with Lingwood's experimental data. This type-3 instability has also been found theoretically in the Ekman boundary layer by Lingwood [13].

It is clear that a comprehensive study of the effect of a compliant wall on the stability of the Ekman flow, or more generally the stability of three-dimensional rotating flow, will require study of the impact on all three types of instability. However, the recent work of Cooper and Carpenter [18,21] have considered in detail the type-1 and type-2 instability [18] and the type-3 instability [21], for the case of the rotating disc with a compliant surface. In this paper, as a starting point, we consider the impact of a compliant surface on the neutral curves of the Ekman flow for the type-2 instability, which is the one occuring at lowest Reynolds number. The results are quite surprising, in that they show a neglible effect on the stability, even with very compliant surfaces. With the same compliant surface properties, the effect on the Blasius boundary layer is significant [22,23]. To be more precise, at moderate-to-high Reynold's number there is a significant wall-compliance effect on neutral curves for the Blasius boundary layer [22], but less so at lower Reynold's number, although the effect on instability growth rates is always more pronounced.

On the other hand, the results found in this paper are consistent with the results obtained by Cooper and Carpenter [18] for type-2 instabilities in the rotating disc. There they found that, in terms of neutral-stability curves, relatively low levels of wall compliance had a strong *destabilizing* effect on the type 2 instability, shifting the critical Reynolds number from a value well above that for the type 1 to a value well below (see Fig. 2 of [18]). For higher levels of wall compliance this destabilizing effect weakened. Evidence that this destabilization is associated with horizontal wall displacement is given in the recent numerical experiments of Davies and Carpenter [20]. There they found that wall compliance (using a Kramer-type compliant surface) has only a very weak effect on the stability of the type 2 disturbances for the von Kármán flow.

An outline of the paper is as follows. In Section 2 the basic equations and Ekman solution are set up, and in Section 3 the hydrodynamic stability problem is set up. Since the Ekman problem is on an unbounded domain, the stability problem will have both discrete and continuous spectra. In Section 4 the continous spectrum is identified following work of [7,9,14], and the implications for the numerical scheme are discussed. The model for the compliant surface is developed in Section 5. The model we use is an extension to two space dimensions of the Kramer-type model first introduced by Carpenter and Garrad [22]. It is effectively the equation for a vibrating plate with a spring term, a tension term and a damping term included, driven by the pressure in the fluid. The parameter values we use in the surface model are the same values used in the results in [22] which are consistent with Kramer's experiments. The coupled stability problem is summarized in Section 6.

Section 7 forms a significant part of the paper. It introduces the numerical framework for the linear stability problem. The three approaches to solving hydrodynamic stability problems numerically in the literature are [24]: (a) matrix methods based on finite-difference or spectral discretizations, (b) shooting with orthogonalization, (c) shooting with the compound matrix method. For eigenvalue problems on infinite domains, matrix methods create a significant number of spurious eigenvalues, due to fracturing of the continuous spectrum, and incorrect boundary conditions must be used to preserve linearity in the spectral parameter. An extreme example where a significant number of spurious eigenvalues is generated (indeed, it appears that the number of spurious eigenvalues tends to infinity as the discretization length tends to zero) is presented in [25].

Method (b), orthogonalization, results in non-analytic solutions [26], and on infinite domains there is the added problem that asymptotically correct boundary conditions may not preserve analyticity. The compound matrix method is clearly the best approach to hydrodynamic stability problems on infinite domains. The approach we use here is motivated by the compound matrix method, which has recently been re-developed using exterior algebra [23]. In addition to making the method coordinate-free (i.e., any basis can be used), the new developments include automation of the construction of induced systems, formulation of boundary conditions, role of analyticity, role of the Grassmannian and the use of geometric integrators for integrating the equations [23]. In Section 7 we give a detailed derivation of the equations and boundary conditions, and the issues associated with analyticity for the case of hydrodynamic stability problems on $\mathbb{C}^6$ with three boundary conditions at $z = 0$ and a three-dimensional subspace of decaying solutions as $z \to \infty$. Rigorous asymptotically correct boundary conditions are derived, and then a new numerical algorithm for setting up the boundary conditions numerically is presented based on an idea suggested in [23]. Sections 8–10 then give results for computed neutral curves, firstly for the case of a rigid wall and then for the case of a compliant surface interacting with a type-2 mode of instability.

2. Three-dimensional rotating flow and the Ekman layer

Consider a boundary layer flow over a rotating flat plate extending infinitely in the stream-wise, x, and spanwise, y, directions with vertical direction z extending from $z = 0$ to $z = \infty$. The plate is represented by the plane $z = 0$, and the axis of rotation is vertical rotating at constant angular velocity Ω.

The governing equations are the continuity equation

$$u_x + v_y + w_z = 0, \tag{2.1}$$

and the Navier–Stokes equations relative to a rotating reference frame [2],

$$\begin{aligned}
&u_t + uu_x + vu_y + wu_z + \frac{1}{R_o}p_x - \frac{2}{R_o}v = \frac{1}{R_e}(u_{xx} + u_{yy}) + \frac{1}{R_o}u_{zz},\\
&v_t + uv_x + vv_y + wv_z + \frac{1}{R_o}p_y + \frac{2}{R_o}u = \frac{1}{R_e}(v_{xx} + v_{yy}) + \frac{1}{R_o}v_{zz},\\
&w_t + uw_x + vw_y + ww_z + \frac{1}{R_o E_k}p_z = \frac{1}{R_e}(w_{xx} + w_{yy}) + \frac{1}{R_o}w_{zz}.
\end{aligned} \tag{2.2}$$

These equations are dimensionless and the non-dimensionalization is as follows, where $*$ values are dimensional,

$$\begin{aligned}
&x = \frac{x^*}{L}, \quad y = \frac{y^*}{L}, \quad z = \frac{1}{\sqrt{E_k}}\frac{z^*}{L}, \quad t = \frac{U_\infty}{L}t^*,\\
&u = \frac{u^*}{U_\infty}, \quad v = \frac{v^*}{U_\infty}, \quad w = \frac{1}{\sqrt{E_k}}\frac{w^*}{U_\infty}, \quad p = \frac{p^*}{\rho\Omega L U_\infty},
\end{aligned} \tag{2.3}$$

where U_∞ is the geostrophic velocity in the farfield, ρ is the fluid density, and the dimensionless parameters are

$$E_k = \frac{\nu}{\Omega L^2}, \quad R_e = \frac{U_\infty L}{\nu} \quad \text{and} \quad R_o = \frac{U_\infty}{\Omega L}. \tag{2.4}$$

The only unusual aspect of this non-dimensionalization is the use of the Ekman number to scale the vertical direction and the vertical velocity field. Indeed, for the rigid wall problem, the Ekman number can be scaled out of the linear stability problem completely (see comments at the end of Section 3). However, when the coupled Ekman-wall problem is considered, the Ekman number no longer disappears. Maintaining the Ekman number allows independent variation of both the rotation rate and the length scale (this is discussed further in Section 9).

The parameter E_k is the Ekman number, R_e is the Reynolds number and R_o is the Rossby number. These three numbers are related by

$$E_k = \frac{R_o}{R_e}.$$

The boundary condition at the surface is the no slip condition (the boundary conditions for a compliant surface will be considered later)

$$u = v = w = 0 \quad \text{at } z = 0.$$

In the farfield, the velocity is asymptotic to the geostrophic velocity field. In dimensionless coordinates, this condition is

$$\lim_{z\to\infty} u(x, y, z, t) = 1 \quad \text{and} \quad \lim_{z\to\infty} v(x, y, z, t) = \lim_{z\to\infty} w(x, y, z, t) = 0.$$

It is straightforward to verify that the full nonlinear problem has an exact solution, the Ekman boundary layer (where p_0 is an arbitrary constant).

$$\begin{aligned}
&u(x, y, z, t) = U(z) = 1 - \mathrm{e}^{-z}\cos z,\\
&v(x, y, z, t) = V(z) = \mathrm{e}^{-z}\sin z,\\
&w(x, y, z, t) = 0,\\
&p(x, y, z, t) = -2y + p_0.
\end{aligned} \tag{2.5}$$

3. Linear stability of the Ekman boundary layer

The Navier–Stokes equations linearized about the Ekman boundary layer take the following form,

$$\begin{aligned}
&u_t + Uu_x + Vu_y + U_z w + \frac{1}{R_o}p_x - \frac{2}{R_o}v = \frac{1}{R_e}(u_{xx}+u_{yy}) + \frac{1}{R_o}u_{zz},\\
&v_t + Uv_x + Vv_y + V_z w + \frac{1}{R_o}p_y + \frac{2}{R_o}u = \frac{1}{R_e}(v_{xx}+v_{yy}) + \frac{1}{R_o}v_{zz},\\
&w_t + Uw_x + Vw_y + \frac{1}{R_o E_k}p_z = \frac{1}{R_e}(w_{xx}+w_{yy}) + \frac{1}{R_o}w_{zz}.
\end{aligned} \tag{3.1}$$

The system is completed by adding the linearized continuity equation $u_x + v_y + w_z = 0$. Introduce a normal-mode form of solution,

$$\begin{pmatrix} u(x,y,z,t)\\ v(x,y,z,t)\\ w(x,y,z,t)\\ p(x,y,z,t)\end{pmatrix} = \begin{pmatrix} \hat{u}(z)\\ \hat{v}(z)\\ \widehat{w}(z)\\ \hat{p}(z)\end{pmatrix} \mathrm{e}^{\mathrm{i}(\alpha x+\beta y-\omega t)} + \text{complex conjugate}. \tag{3.2}$$

The phase speed for the waves is defined by $c = \omega/\gamma$ where $\gamma^2 = \alpha^2 + \beta^2$. Substitution of the normal-mode solution into the linearized equations (3.1) and the continuity equation leads to

$$\begin{aligned}
&\mathrm{i}\alpha\hat{u} + \mathrm{i}\beta\hat{v} + \widehat{w}_z = 0,\\
&\mathrm{i}\gamma R_o\left(\frac{\alpha}{\gamma}U + \frac{\beta}{\gamma}V - c\right)\hat{u} + R_o U_z\widehat{w} + \mathrm{i}\alpha\hat{p} - 2\hat{v} = \hat{u}_{zz} - \gamma^2 E_k\hat{u},\\
&\mathrm{i}\gamma R_o\left(\frac{\alpha}{\gamma}U + \frac{\beta}{\gamma}V - c\right)\hat{v} + R_o V_z\widehat{w} + \mathrm{i}\beta\hat{p} + 2\hat{u} = \hat{v}_{zz} - \gamma^2 E_k\hat{v},\\
&\mathrm{i}\gamma R_o\left(\frac{\alpha}{\gamma}U + \frac{\beta}{\gamma}V - c\right)\widehat{w} + \hat{p}_z = \widehat{w}_{zz} - \gamma^2 E_k\widehat{w}.
\end{aligned} \tag{3.3}$$

These equations can be simplified by using a rotated velocity field. Let

$$\begin{aligned}
&\widetilde{U} = \frac{\alpha}{\gamma}U + \frac{\beta}{\gamma}V, \qquad \tilde{u} = \frac{\alpha}{\gamma}\hat{u} + \frac{\beta}{\gamma}\hat{v},\\
&\widetilde{V} = \frac{\beta}{\gamma}U - \frac{\alpha}{\gamma}V, \qquad \tilde{v} = \frac{\beta}{\gamma}\hat{u} - \frac{\alpha}{\gamma}\hat{v},
\end{aligned} \tag{3.4}$$

then the governing equations simplify to

$$\begin{aligned}
&\mathrm{i}\gamma\tilde{u} + \widehat{w}_z = 0,\\
&\mathrm{i}\gamma R_o\big(\widetilde{U} - c\big)\tilde{u} + R_o\widetilde{U}_z\widehat{w} + \mathrm{i}\gamma\hat{p} + 2\tilde{v} = \tilde{u}_{zz} - \gamma^2 E_k\tilde{u},\\
&\mathrm{i}\gamma R_o\big(\widetilde{U} - c\big)\tilde{v} + R_o\widetilde{V}_z\widehat{w} - 2\tilde{u} = \tilde{v}_{zz} - \gamma^2 E_k\tilde{v},\\
&\mathrm{i}\gamma R_o\big(\widetilde{U} - c\big)\widehat{w} + \hat{p}_z = \widehat{w}_{zz} - \gamma^2 E_k\widehat{w}.
\end{aligned} \tag{3.5}$$

The second equation can be solved for the pressure. Substitution of the pressure into the fourth equation reduces the system to a pair of coupled ODEs for $\widehat{w}$ and $\tilde{v}$. Given $\widehat{w}$ and $\tilde{v}$, $\tilde{u}$ is then obtained from the third equation of (3.5). Let

$$\phi(z) = \widehat{w}(z) \quad \text{and} \quad \psi(z) = \mathrm{i}\gamma\tilde{v}(z),$$

then the governing equations for ϕ and ψ are

$$\begin{aligned}
&\mathbf{M}^2\phi - \mathrm{i}\gamma R_o\big(\widetilde{U} - c\big)\mathbf{M}\phi + \mathrm{i}\gamma R_o\widetilde{U}_{zz}\phi + 2\psi_z = 0,\\
&\mathbf{M}\psi - \mathrm{i}\gamma R_o\big(\widetilde{U} - c\big)\psi - \mathrm{i}\gamma R_o\widetilde{V}_z\phi - 2\phi_z = 0
\end{aligned} \tag{3.6}$$

with $\mathbf{M}\phi := \phi_{zz} - \gamma^2 E_k\phi$ and boundary conditions

$$\phi(0) = \psi(0) = \phi_z(0) = 0 \quad \text{and} \quad \phi, \phi_z, \psi \to 0 \quad \text{as } z \to \infty.$$

If E_k is set equal to unity, $R_o = R_e$, and these equations reduce exactly to those of Lilly [4].

It will be useful to express the wavenumber vector (α, β) in polar coordinates,

$$\alpha = -\gamma \sin\varepsilon \quad \text{and} \quad \beta = \gamma \cos\varepsilon. \tag{3.7}$$

The rotated velocity field can then be written in the form

$$\begin{aligned} \widetilde{U} &= -\sin\varepsilon\big(1 - \mathrm{e}^{-z}\cos z\big) + \cos\varepsilon\,\mathrm{e}^{-z}\sin z, \\ \widetilde{V} &= \cos\varepsilon\big(1 - \mathrm{e}^{-z}\cos z\big) + \sin\varepsilon\,\mathrm{e}^{-z}\sin z. \end{aligned} \tag{3.8}$$

It is tempting to scale out the Ekman number from the linear stability equations (3.6). With the substitution

$$\tilde{\gamma} = \gamma\sqrt{E_k} \quad \text{and} \quad \widetilde{R}_o = R_o/\sqrt{E_k},$$

the Ekman number is eliminated from (3.6) and the boundary conditions. However, when the compliant wall is added the boundary conditions change, and it does not appear to be possible to scale away the Ekman number.

4. Continuous spectra and the system at infinity

In this section, more precise boundary conditions at infinity are derived. These boundary conditions are affected by the position of the continuous spectrum. As is typical of stability problems on unbounded domains [9], the Ekman problem has a branch of continuous spectrum. This spectrum can be determined by studying the system (3.6) in the limit $z \to \infty$, the "system at infinity".

The z-dependent coefficients of the ODE (3.6) decay exponentially to constant values as $z \to \infty$. Therefore "system at infinity" is

$$\begin{aligned} &\left(\frac{\mathrm{d}^2}{\mathrm{d}z^2} - \gamma^2 E_k\right)^2 \phi - \mathrm{i}\gamma R_o\big(\widetilde{U}_\infty - c\big)\left(\frac{\mathrm{d}^2}{\mathrm{d}z^2} - \gamma^2 E_k\right)\phi + 2\psi_z = 0, \\ &\left(\frac{\mathrm{d}^2}{\mathrm{d}z^2} - \gamma^2 E_k\right)\psi - \mathrm{i}\gamma R_o\big(\widetilde{U}_\infty - c\big)\psi - 2\phi_z = 0. \end{aligned} \tag{4.1}$$

The general solution can be expressed as a sum of exponentials. Let $\phi(z) = \mathrm{e}^{\mu z}\hat{\phi}$ and $\psi(z) = \mathrm{e}^{\mu z}\hat{\psi}$ where μ is in general complex and $(\hat{\phi}, \hat{\psi}, \mu)$ satisfy the "nonlinear in the parameter" eigenvalue problem

$$\begin{bmatrix} (\mu^2 - \gamma^2 E_k)^2 - \Lambda(\mu^2 - \gamma^2 E_k) & 2\mu \\ -2\mu & (\mu^2 - \gamma^2 E_k) - \Lambda \end{bmatrix} \begin{pmatrix} \hat{\phi} \\ \hat{\psi} \end{pmatrix} = 0, \tag{4.2}$$

where

$$\Lambda = \mathrm{i}\gamma R_o\big(\widetilde{U}_\infty - c\big) = \mathrm{i}\gamma R_o\left(\widetilde{U}_\infty - \mathrm{i}\frac{\lambda}{\gamma}\right) = \mathrm{i}\gamma R_o\left(\frac{\alpha}{\gamma} - \mathrm{i}\frac{\lambda}{\gamma}\right) = R_o(\lambda + \mathrm{i}\alpha)$$

using $\lambda = -\mathrm{i}\gamma c$ and

$$\widetilde{U}_\infty = \lim_{z\to\infty} \widetilde{U}(z) = \lim_{z\to\infty}\left[\frac{\alpha}{\gamma}U(z) + \frac{\beta}{\gamma}V(z)\right] = \frac{\alpha}{\gamma}.$$

The eigenvalue problem (4.2) has a nontrivial solution if and only if the determinant of the coefficient matrix, $\Delta(\mu, \lambda)$, vanishes where

$$\begin{aligned} \Delta(\mu,\lambda) &= \det\begin{bmatrix} (\mu^2 - \gamma^2 E_k)^2 - \Lambda(\mu^2 - \gamma^2 E_k) & 2\mu \\ -2\mu & (\mu^2 - \gamma^2 E_k) - \Lambda \end{bmatrix} \\ &= \big(\mu^2 - \gamma^2 E_k\big)\big(\mu^2 - \gamma^2 E_k - \Lambda\big)^2 + 4\mu^2 \\ &= \mu^6 - f_1\mu^4 + f_2\mu^2 - f_3 \end{aligned} \tag{4.3}$$

with

$$f_1 = 3\gamma^2 E_k + 2R_o(\lambda + \mathrm{i}\alpha), \tag{4.4}$$

$$f_2 = 4 + 3\gamma^4 E_k^2 + 4\gamma^2 E_k R_o(\lambda + \mathrm{i}\alpha) + R_o^2(\lambda + \mathrm{i}\alpha)^2, \tag{4.5}$$

$$f_3 = \gamma^2 E_k\big(\gamma^2 E_k + R_o(\lambda + \mathrm{i}\alpha)\big)^2. \tag{4.6}$$

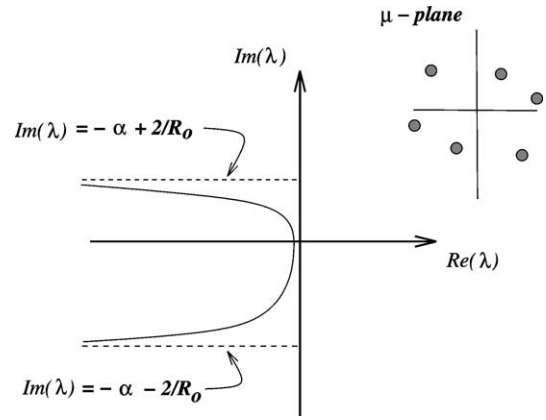

Fig. 2. A schematic of the position of the continuous spectrum of the Ekman hydrodynamic stability problem when $E_k = 1$, and a schematic of the position of the μ-eigenvalues when λ lies to the right of the continuous spectrum.

A solution of (4.1) is exponentially decaying as $z \to +\infty$ if $\mathrm{Re}(\mu) < 0$ and exponentially growing as $z \to +\infty$ if $\mathrm{Re}(\mu) > 0$. The continuous spectrum, where $\mathrm{Re}(\mu) = 0$, separates these two regions,

$$\sigma_c = \{\lambda \in \mathbb{C}\colon\ \Delta(\mathrm{i}k, \lambda) = 0,\ k \in \mathbb{R}\}.$$

The continuous spectrum of the Ekman problem is well known [7,9,14] and, using the present notation, it can be expressed in the form

$$\sigma_c = \left\{\lambda \in \mathbb{C}\colon\ \mathrm{Re}(\lambda) = -\frac{\gamma^2 E_k + k^2}{R_o},\ \mathrm{Im}(\lambda) = -\alpha + \frac{2k}{R_o\sqrt{\gamma^2 E_k + k^2}},\ k \in \mathbb{R}\right\},$$

and a schematic of the continuous spectrum is shown in Fig. 2.

If $\lambda \notin \sigma_c$, then any $\mu \in \mathbb{C}$ satisfying $\Delta(\mu, \lambda)$ will have nonzero real part. Therefore, for any $\lambda \in \mathbb{C}$ with $\mathrm{Re}(\lambda) > 0$, it is clear that $\Delta(\mu, \lambda) = 0$ has six complex roots all of which have non-zero real parts. It is not difficult to show that three of these have positive real part and three have negative real part [7,9,14]. A schematic of the position of the μ-roots of $\Delta = 0$ for all λ with $\mathrm{Re}(\lambda) > 0$ is shown in Fig. 2.

Henceforth we assume that $\mathrm{Re}(\lambda) > -(\gamma^2/R_o)E_k$ and let μ_1, μ_2 and μ_3 be the three roots of $\Delta(\mu, \lambda) = 0$ with positive real part, and let μ_4, μ_5 and μ_6 be the three roots with negative real part. Then it is clear, that any solution of (3.6) which is bounded as $z \to \infty$ has to be asymptotic to a linear combination of the eigenvectors associated with μ_4, μ_5 and μ_6. The most natural way to formulate this is in terms of the eigenvectors associated with μ_1, μ_2 and μ_3 and this will be done in Section 6.

5. Modelling the compliant surface

The compliant surface is modelled using a generalization of the Kramer-type model introduced by Carpenter and Garrad [22], extended for a two-dimensional plate adjacent to a three-dimensional fluid. The Kramer-type compliant surface is a simple plate-spring surface-based model. It is assumed to be constructed of an elastic plate (or tensioned membrane) supported above a rigid surface by a vertically aligned array of springs. A schematic of the model is shown in Fig. 3. The various parameters characterising the surface properties are estimated for the actual Kramer coatings using data reported in [22] (see Section 9 for actual data). The only new parameter which does not appear in [22] is the rotation rate Ω, but this will be expressed in terms of known parameters and the Ekman number.

This type of model is an idealistic representation for the wall and is not an accurate representation for all the types of wall used in experimental studies [3]. Nevertheless, it is a start enabling us to estimate what effect wall compliance may have on Tollmien–Schlichting type instabilities in rotating boundary layers. This model for the wall has the advantage of leading to a problem which is computationally efficient.

After non-dimensionalizing and linearizing, the kinematic condition at the surface, that is, the surface velocity equals the fluid velocity, takes the form

$$u + U_z(0)\zeta = 0, \quad v + V_z(0)\zeta, \quad w = \zeta_t \quad \text{at } z = 0.$$

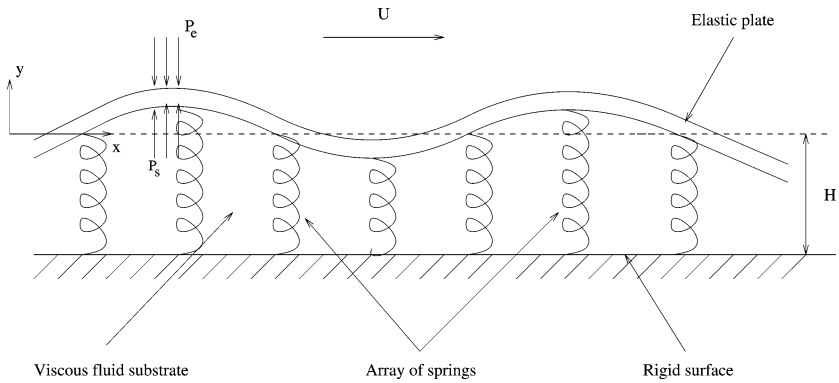

Fig. 3. A schematic illustration of the theoretical model for a compliant surface.

In the derivation, the rate of change of deformations in the plate surface are neglected [27], and ζ, the vertical surface displacement, is made dimensionless in the same way as the vertical coordinate z. Eliminating ζ from the first two equations, introducing normal mode form with rotated coordinates leads to a boundary condition in terms of ϕ and ψ

$$\widetilde{U}_z\psi + \widetilde{V}_z\phi_z = 0 \quad \text{at } z = 0. \tag{5.1}$$

With the normal-mode ansatz, $\hat{u}$ and $\hat{v}$ can be expressed in terms of $\widehat{w}$: $\mathrm{i}\gamma c\hat{u} = U_z(0)\widehat{w}$, $\mathrm{i}\gamma c\hat{v} = V_z(0)\widehat{w}$. Combining these expressions with the continuity equation leads to the second boundary condition

$$c\phi_z + \widetilde{U}_z(0)\phi = 0 \quad \text{at } z = 0. \tag{5.2}$$

Setting up the dynamic condition is a little more work. After non-dimensionalization, the dynamic equation of the wall is

$$C_m\zeta_{tt} + C_d\zeta_t + C_B\Delta^2\zeta - C_T\Delta\zeta + C_{KE}\zeta = -E_k^{-3/2}R_e^{-1}p_{\text{wall}}(x, y, t), \tag{5.3}$$

where $\Delta = \partial_x^2 + \partial_y^2$ and

$$C_m = \frac{\rho_m}{\rho}\frac{U_\infty b}{\nu}R_e^{-1}, \quad C_d = \frac{d}{\rho U_\infty}, \quad C_B = \frac{BU_\infty}{\rho\nu^3}R_e^{-3}, \quad C_T = \frac{T}{\rho U_\infty \nu}R_e^{-1}, \quad C_{KE} = \frac{\nu k_E}{\rho u_\infty^3}R_e. \tag{5.4}$$

Eq. (5.3) is a straightforward generalization of the dynamic equation in [22] to two space dimensions. Note that the dimensionless parameters take the same form as in [22]. The rotation rate appears here in the Ekman number multiplying the pressure. If we set $E_k = 1$ and neglect spanwise variation $\partial_y = 0$, the equation for the wall reduces exactly to the equation used in [22] (when the substrate is neglected).

The dimensionless numbers R_e and E_k appear because L and Ω have been eliminated in terms of them,

$$L = \frac{\nu R_e}{U_\infty} \quad \text{and} \quad \Omega = \frac{\nu}{E_k L^2} = \frac{U_\infty^2}{\nu E_k R_e^2}.$$

The dimensional parameters have the following definition: ρ_m is the material density, ρ is the fluid density, b is the plate thickness, ν is the fluid kinematic viscosity, U_∞ is the farfield geostrophic velocity, d is a material damping parameter, B is the bulk modulus of the material, T is the material tension parameter, k_E is a spring constant for the spring backing the plate, and p_{wall} is the fluid pressure acting on the plate.

Normal mode substitution, and use of the relation between $\hat{\zeta}$ and $\widehat{w}$, leads to the following form of (5.3)

$$\mathrm{i}\gamma c\hat{p}_{\text{wall}} + E_k^{3/2}R_e\Gamma\widehat{w} = 0 \quad \text{at } z = 0, \tag{5.5}$$

where

$$\Gamma = \gamma^2c^2C_M + \mathrm{i}\gamma cC_d - C_B\gamma^4 - C_T\gamma^2 - C_{KE}. \tag{5.6}$$

This third boundary condition is completed by substituting an expression for the pressure at the wall. The pressure $\hat{p}_{\text{wall}}$ is obtained by evaluating the second equation of (3.5) at $z = 0$ and then replacing $\tilde{u}$ with $\widehat{w}$ using the continuity equation resulting in

$$\hat{p}_{\text{wall}} = \frac{1}{\gamma^2}\left(\phi_{zzz} - \gamma^2E_k\phi_z + 2\psi\right) \quad \text{at } z = 0. \tag{5.7}$$

Combining this expression with (5.5) leads to the final form for the dynamic boundary condition

$$\mathrm{i}c\big(\phi_{zzz} - \gamma^2 E_k \phi_z + 2\psi\big) + \gamma E_k^{3/2} R_e \Gamma \phi = 0 \quad \text{at } z = 0. \tag{5.8}$$

When $\psi = 0$ and $E_k = 1$, this condition reduces exactly to the boundary condition for a compliant surface interacting with the Blasius boundary layer (cf. Eqs. (4.9), (4.12) and (6.5) in [22], §11.1.2, §14.2 and Eq. (11.5) in [27] and Eq. (7.2) in [23]).

In summary the three boundary conditions for (3.6) at $z = 0$ due to the compliant surface are the two kinematic conditions (5.1) and (5.2) and the dynamic condition (5.8).

6. The stability problem for an Ekman layer interacting with a compliant wall

In this section, the hydrodynamic stability problem is put into a canonical form for the numerical framework to be introduced in Section 7. First Eqs. (3.6) are put into the standard form of a first-order system. Introduce the vector

$$\mathbf{u}(z,\lambda) = \big(u_1(z,\lambda), \ldots, u_6(z,\lambda)\big) \in \mathbb{C}^6,$$

where the components of $\mathbf{u}$ are defined by

$$u_1 = \phi, \quad u_2 = \phi_z, \quad u_3 = \phi_{zz}, \quad u_4 = \phi_{zzz}, \quad u_5 = \psi, \quad u_6 = \psi_z.$$

Then this vector satisfies

$$\mathbf{u}_z = \mathbf{A}(z,\lambda)\mathbf{u}, \quad \mathbf{u} \in \mathbb{C}^6,\ \lambda \in \mathbb{C}, \tag{6.1}$$

where

$$\mathbf{A}(z,\lambda) = \begin{bmatrix} 0 & 1 & 0 & 0 & 0 & 0 \\ 0 & 0 & 1 & 0 & 0 & 0 \\ 0 & 0 & 0 & 1 & 0 & 0 \\ -a(z,\lambda) & b(z,\lambda) & 0 & 0 & 0 & -2 \\ 0 & 0 & 0 & 0 & 0 & 1 \\ \mathrm{i}\gamma R_o \widetilde{V}_z & 2 & 0 & 0 & b(z,\lambda) - \gamma^2 E_k & 0 \end{bmatrix}, \tag{6.2}$$

with

$$\begin{aligned} a(z,\lambda) &= \gamma^4 E_k^2 + \mathrm{i}\gamma^2 R_o E_k\big(\gamma\widetilde{U} - \mathrm{i}\lambda\big) + \mathrm{i}\gamma R_o \widetilde{U}_{zz} + \mathrm{i}R_o\big(\gamma\widetilde{U} - \mathrm{i}\lambda\big), \\ b(z,\lambda) &= 2\gamma^2 E_k + \mathrm{i}R_o\big(\gamma\widetilde{U} - \mathrm{i}\lambda\big). \end{aligned} \tag{6.3}$$

In terms of the vector $\mathbf{u}$ the boundary conditions at $z = 0$, associated with the compliant surface (5.1), (5.2), (5.8), can be expressed in the form

$$\mathbf{a}_j(\lambda) \cdot \mathbf{u}(z,\lambda)|_{z=0} = 0, \quad j = 1,2,3, \tag{6.4}$$

where

$$\mathbf{a}_1(\lambda) = \begin{pmatrix} \cos\varepsilon - \sin\varepsilon \\ \mathrm{i}\lambda/\gamma \\ 0 \\ 0 \\ 0 \\ 0 \end{pmatrix}, \quad \mathbf{a}_2(\lambda) = \begin{pmatrix} 0 \\ \cos\varepsilon + \sin\varepsilon \\ 0 \\ 0 \\ \cos\varepsilon - \sin\varepsilon \\ 0 \end{pmatrix}, \quad \mathbf{a}_3(\lambda) = \begin{pmatrix} \gamma^2 E_k^{3/2} \\ \gamma^2 \lambda E_k/(R_e\Gamma) \\ 0 \\ -\lambda/(R_e\Gamma) \\ -2\lambda/(R_e\Gamma) \\ 0 \end{pmatrix}.$$

The product in (6.4) is the usual dot product but without complex conjugation. (If a Hermitian inner product is used, the vector $\mathbf{a}_j(\lambda)$ is just replaced with $\overline{\mathbf{a}_j(\lambda)}$.)

The three boundary conditions (6.4) are not independent for all values of the parameters. For example, when $\lambda = 0$ it is easily seen that $\mathbf{a}_1(\lambda)$ is a multiple of $\mathbf{a}_3(\lambda)$. Therefore these boundary conditions are not valid for $\lambda = 0$. When $\lambda \neq 0$, it is easy to check that the boundary conditions are independent if $\cos\varepsilon - \sin\varepsilon \neq 0$. Therefore we will assume henceforth that

$$\lambda(\cos\varepsilon - \sin\varepsilon) \neq 0. \tag{6.5}$$

In the limit as the compliant surface approaches a rigid wall, the boundary conditions (6.4) should reduce to the rigid-wall conditions. The rigid wall limit appears in the boundary conditions as $|\Gamma| \to \infty$. This limit is the reason that Γ is

placed in the denominator in the vector $\mathbf{a}_3(\lambda)$. Then, in the limit as $|\Gamma| \to \infty$ the boundary conditions $\mathbf{a}_1(\lambda) \cdot \mathbf{u}(0,\lambda) = 0$ and $\mathbf{a}_3(\lambda) \cdot \mathbf{u}(0,\lambda) = 0$ reduce to $\phi(0) = \phi'(0) = 0$. And then, with (6.5), $\mathbf{a}_2(\lambda) \cdot \mathbf{u}(0,\lambda) = 0$ reduces to $\psi(0) = 0$. Therefore, the rigid wall limit is a well-defined limit of the boundary conditions (6.4).

We now turn to the boundary conditions to be applied at $z = L_\infty$ where L_∞ is some large value of z. The idea is to derive asymptotically correct boundary conditions. They are derived using properties of the system at infinity (4.1).

In terms of the system (6.1), the system at infinity is $\mathbf{u}_x = \mathbf{A}_\infty(\lambda)\mathbf{u}$ where

$$\mathbf{A}_\infty(\lambda) = \lim_{z\to\infty} \mathbf{A}(z,\lambda),$$

and

$$\det\big[\mu\mathbf{I} - \mathbf{A}_\infty(\lambda)\big] = \Delta(\mu,\lambda),$$

where $\Delta(\mu,\lambda)$ is the characteristic polynomial defined in (4.3). Let $\eta_j(\lambda)$, $j = 1,2,3$, be the adjoint eigenvectors of $\mathbf{A}_\infty(\lambda)$ associated with the eigenvalues μ_j, $j = 1,2,3$, which have positive real part,

$$\eta_j(\lambda)^*\big[\mathbf{A}_\infty(\lambda) - \mu_j\mathbf{I}\big] = \mathbf{0} \quad \text{or} \quad \big[\mathbf{A}_\infty(\lambda)^* - \overline{\mu_j}\mathbf{I}\big]\eta_j(\lambda) = 0.$$

Note that each $\eta_j(\lambda)$ is not an analytic function, but $\overline{\eta_j(\lambda)}$ is analytic. Therefore, define

$$\mathbf{b}_j(\lambda) = \overline{\eta_j(\lambda)}, \quad j = 1,2,3.$$

Then, the appropriate boundary conditions at $z = L_\infty$ are

$$\mathbf{b}_j(\lambda) \cdot \mathbf{u}(z,\lambda)|_{z=L_\infty} = 0, \quad j = 1,2,3. \tag{6.6}$$

It is not difficult to show that these boundary conditions are asymptotically exact [28,29] *for each fixed* λ. However, if any of the $\{\mu_1,\mu_2,\mu_3\}$ coalesce then these boundary conditions may become singular. The eigenvalues coalesce when $\Delta(\mu,\lambda) = \Delta_\mu(\mu,\lambda) = 0$. This pair of equations reduces to a quartic for λ. Therefore in general one can expect four points in the λ plane where eigenvalues in the set $\{\mu_1,\mu_2,\mu_3\}$ coalesce. This difficulty is a fundamental problem with the use of individual eigenvectors. However, this difficulty will disappear when the stability problem is formulated on $\bigwedge^3(\mathbb{C}^6)$ in Section 7. The reason is that the subspace $\text{span}\{\eta_1(\lambda),\eta_2(\lambda),\eta_3(\lambda)\}$ is analytic even though individual eigenvectors may not be analytic. On $\bigwedge^3(\mathbb{C}^6)$ the three-dimensional subspaces of $\mathbb{C}^6$ are points and therefore the problem disappears.

In summary, the linear stability of the Ekman layer coupled to a compliant surface reduces to solving the ODE (6.1) subject to the three boundary conditions (6.4) at $z = 0$ and the three asymptotic boundary conditions (6.6) at $z = L_\infty$, with the exact problem obtained in the limit $L_\infty \to \infty$.

7. Numerical integration of ODEs on $\bigwedge^3(\mathbb{C}^6)$

This section is effectively independent of the rest of the paper. Notation from the rest of the paper will be used for consistency, but the algorithm will be described in general terms.

The problem is to integrate a linear system of ODEs on $\mathbb{C}^6$ which are defined on an interval $z \in [0,\infty]$ with three boundary conditions at $z = 0$ and three asymptotic boundary conditions applied at $z = L_\infty$ for some $L_\infty > 0$. The ODE takes the standard form

$$\mathbf{u}_x = \mathbf{A}(z,\lambda)\mathbf{u}, \quad \mathbf{u} \in \mathbb{C}^6, \tag{7.1}$$

with $\mathbf{A}(z,\lambda)$ a smooth function of z (at least continuously differentiable) and an analytic function of λ for all λ in some open subset of the λ plane. The matrix $\mathbf{A}_\infty(\lambda)$, defined in the usual way, is assumed to exist and to have a 3–3 splitting: three eigenvalues with negative real part and three with positive real part for all λ of interest.

The boundary conditions at $z = 0$ take the form (6.4) with each $\mathbf{a}_j(\lambda)$ an analytic function, and the boundary conditions at $z = L_\infty$ take the form (6.6). Even though the individual vectors $\mathbf{b}_j(\lambda)$ may not be analytic for all λ of interest, this will not be important in the algorithm, because *the induced boundary condition on* $\bigwedge^3(\mathbb{C}^6)$ *will be analytic* [23].

7.1. The induced ODE on $\bigwedge^3(\mathbb{C}^6)$

The boundary condition at $z = L_\infty$ defines a three-dimensional subspace of $\mathbb{C}^6$ and the boundary condition at $z = 0$ defines a second three-dimensional subspace of $\mathbb{C}^6$. Therefore the problem reduces to finding a path of three-dimensional subspaces which satisfy (7.1) which link the two boundary subspaces. A subspace spanned by three linearly independent vectors such as $\{\mathbf{a}_1,\mathbf{a}_2,\mathbf{a}_3\}$ can be represented as a point $\mathbf{a}_1 \wedge \mathbf{a}_2 \wedge \mathbf{a}_3$ in the larger vector space $\bigwedge^3(\mathbb{C}^6)$, where $\wedge$ is the wedge product.

Let $\mathbf{e}_1, \ldots, \mathbf{e}_6$ be a basis for $\mathbb{C}^6$, then the set of all nonzero elements $\mathbf{e}_i \wedge \mathbf{e}_j \wedge \mathbf{e}_k$ form a basis for $\bigwedge^3(\mathbb{C}^6)$. The dimension of $\bigwedge^3(\mathbb{C}^6)$ is $\frac{6!}{3!3!} = 20$. A basis for $\bigwedge^3(\mathbb{C}^6)$ is then formed by taking a standard lexicographical ordering,

$$\theta_1 = \mathbf{e}_1 \wedge \mathbf{e}_2 \wedge \mathbf{e}_3,\ \theta_2 = \mathbf{e}_1 \wedge \mathbf{e}_2 \wedge \mathbf{e}_4, \ldots, \theta_{20} = \mathbf{e}_4 \wedge \mathbf{e}_5 \wedge \mathbf{e}_6.$$

In terms of this basis, any $\mathbf{U} \in \bigwedge^3(\mathbb{C}^6)$ can be expressed as

$$\mathbf{U} = \sum_{j=1}^{20} U_j \theta_j.$$

Given *any* basis for $\mathbb{C}^6$ there is then a standard procedure for constructing the induced system on $\bigwedge^3(\mathbb{C}^6)$ [23]. The induced system can be written

$$\mathbf{U}_z = \mathbf{A}^{(3)}(z, \lambda)\mathbf{U}, \quad \mathbf{U} \in \bigwedge^3\big(\mathbb{C}^6\big) \cong \mathbb{C}^{20}, \tag{7.2}$$

where $\mathbf{A}^{(3)}(z, \lambda)$ is a 20×20 matrix. If we take the standard basis for $\mathbb{C}^6$, then the form of the induced matrix on $\bigwedge^3(\mathbb{C}^6)$ is given in the Appendix. The induced system (7.2) will be integrated numerically from $z = L_\infty$ to $z = 0$.

7.2. The initial conditions at $z = L_\infty$

The asymptotic boundary conditions at $z = L_\infty$ define a three-dimensional subspace of $\mathbb{C}^6$. Let $\xi_1(\lambda)$, $\xi_2(\lambda)$ and $\xi_3(\lambda)$ be a basis for this space:

$$\operatorname{span}\big\{\xi_1(\lambda), \xi_2(\lambda), \xi_3(\lambda)\big\} = \big\{\mathbf{u} \in \mathbb{C}^6\colon\ \mathbf{b}_1(\lambda) \cdot \mathbf{u} = \mathbf{b}_2(\lambda) \cdot \mathbf{u} = \mathbf{b}_3(\lambda) \cdot \mathbf{u} = 0\big\}.$$

When the eigenvalues $\{\mu_4, \mu_5, \mu_6\}$ are distinct, the vectors $\xi_1(\lambda)$, $\xi_2(\lambda)$ and $\xi_3(\lambda)$ are just the eigenvectors corresponding to the eigenvalues of $\mathbf{A}_\infty(\lambda)$ with negative real part.

The natural starting vector for the integration of (7.2) is any nonzero multiple of $\xi_1(\lambda) \wedge \xi_2(\lambda) \wedge \xi_3(\lambda) \in \bigwedge^3(\mathbb{C}^6)$. This approach is effectively the one proposed by Ng and Reid [30] to be used with the compound matrix solution of the Orr–Sommerfeld equation on a semi-infinite interval.

This approach has two problems. Firstly, it is not in general possible to construct this basis in such a way that it is analytic for all λ of interest. For example, at certain values of λ eigenvalues in the set $\{\mu_1, \mu_2, \mu_3\}$ may coalesce causing singularities. Secondly each eigenvector would need to be computed, and then combined using the wedge product to get the starting vector. Both problems are eliminated by working directly on $\bigwedge^3(\mathbb{C}^6)$.

Taking the limit $z \to \infty$ of $\mathbf{A}^{(3)}(z, \lambda)$ leads to a matrix $\mathbf{A}^{(3)}_\infty(\lambda)$ which is just the induced matrix associated with $\mathbf{A}_\infty(\lambda)$ [23]. Moreover, the eigenvalues of $\mathbf{A}^{(3)}_\infty(\lambda)$ are just the set of positive three-fold sums of the eigenvalues of $\mathbf{A}_\infty(\lambda)$. Therefore, since there are exactly three eigenvalues of $\mathbf{A}_\infty(\lambda)$ with negative real part, there is a unique simple eigenvalue of $\mathbf{A}^{(3)}_\infty(\lambda)$ of largest negative real part. Denote this eigenvalue by $\sigma_+(\lambda)$ and its eigenvector by $\zeta_+(\lambda)$,

$$\big[\mathbf{A}^{(3)}_\infty(\lambda) - \sigma_+(\lambda)\mathbf{I}_{20}\big]\zeta_+(\lambda) = 0. \tag{7.3}$$

The vector $\zeta_+(\lambda)$ is a constant multiple of $\xi_1(\lambda) \wedge \xi_2(\lambda) \wedge \xi_3(\lambda)$, but the way it is constructed, it will be analytic for all λ away from the continuous spectrum. The matrix $\mathbf{A}^{(3)}_\infty(\lambda)$ is a 20×20 matrix and in general its eigenvalues will have to be found numerically.

Therefore the strategy is as follows for fixed λ: construct $\mathbf{A}^{(3)}_\infty(\lambda)$ and compute numerically all its eigenvalues using a global solver (e.g., QR method); pick out the eigenvalue $\sigma_+(\lambda)$ of largest negative real part, and compute its eigenvector $\zeta_+(\lambda)$. This eigenvector is then the starting vector for the integration

$$\mathbf{U}_x = \mathbf{A}^{(3)}(z, \lambda)\mathbf{U}, \quad L_\infty < z < 0, \quad \mathbf{U}(z, \lambda)|_{z=L_\infty} = \zeta_+(\lambda).$$

However, this algorithm is only for a fixed λ. *It is not analytic as we vary* λ. For example, solve (7.3) for two fixed values, say λ_0 and $\lambda_0 + h$, numerically. What is the limit

$$\lim_{h \to 0} \frac{\zeta_+(\lambda_0 + h) - \zeta_+(\lambda_0)}{h}?$$

Since $\zeta_+(\lambda_0 + h)$ and $\zeta_+(\lambda_0)$ are computed independently, and there is no natural scaling of eigenvectors when computing numerically, this limit will not in general exist. In other words, the numerical continuation will not be analytic. A second issue that arises is that the derivative of $\zeta_+(\lambda)$ will be needed for a Newton algorithm. Both of these issues are solved by constructing an analytic ODE for $\zeta_+(\lambda)$, extending a similar construction in Section 6 of [23] (see also [31]).

Differentiate (7.3) with respect to λ,

$$\big(\mathbf{A}_\infty^{(3)}(\lambda)-\sigma_+(\lambda)\mathbf{I}\big)\frac{\mathrm{d}}{\mathrm{d}\lambda}\zeta_+(\lambda)=-\mathbf{A}_\infty^{(3)\prime}(\lambda)\zeta_+(\lambda)+\sigma_+'(\lambda)\zeta_+(\lambda). \tag{7.4}$$

To obtain $\frac{\mathrm{d}}{\mathrm{d}\lambda}\zeta_+(\lambda)$, it is necessary to solve this system. However, the matrix $(\mathbf{A}_\infty^{(3)}(\lambda)-\sigma_+(\lambda)\mathbf{I}_{20})$ is singular since $\sigma_+(\lambda)$ is an eigenvalue and so, by construction its determinant vanishes.

The idea is to reformulate this system in a way that it can be solved numerically. First, note that a necessary and sufficient condition for the singular equation

$$\big(\mathbf{A}_\infty^{(3)}(\lambda)-\sigma_+(\lambda)\mathbf{I}_{20}\big)\frac{\mathrm{d}}{\mathrm{d}\lambda}\zeta_+(\lambda)=\mathbf{f}$$

to be solvable is that

$$\langle\eta_+(\lambda),\mathbf{f}\rangle_{\mathbb{C}}=0,$$

where $\eta_+(\lambda)$ is the left eigenvector associated with the eigenvalue $\sigma_+(\lambda)$, and $\langle\cdot,\cdot\rangle_{\mathbb{C}}$ is the standard Hermitian inner product on $\mathbb{C}^{20}$. Application to (7.4) shows that $\sigma_+'(\lambda)$ should satisfy

$$\frac{\mathrm{d}}{\mathrm{d}\lambda}\sigma_+(\lambda)=\frac{\langle\eta_+(\lambda),\mathbf{A}_\infty^{(3)\prime}(\lambda)\zeta_+(\lambda)\rangle_{\mathbb{C}}}{\langle\eta_+(\lambda),\zeta_+(\lambda)\rangle_{\mathbb{C}}}.$$

The idea is to reformulate (7.4) as an augmented system on $\mathbb{C}^{21}$:

$$\begin{bmatrix}(\mathbf{A}_\infty^{(3)}(\lambda)-\sigma_+(\lambda)\mathbf{I}) & -\zeta_+(\lambda)\\ -\eta_+(\lambda)^* & 0\end{bmatrix}\begin{pmatrix}\zeta_+'(\lambda)\\ \sigma_+'(\lambda)\end{pmatrix}=\begin{pmatrix}-\mathbf{A}_\infty^{(3)\prime}(\lambda)\zeta_+(\lambda)\\ 0\end{pmatrix}. \tag{7.5}$$

Solving this system yields both $\zeta_+'(\lambda)$ and $\sigma_+'(\lambda)$.

Solving this system for fixed λ provides the derivative which is used in the Newton algorithm below. It is not difficult to show [23] that the coefficient matrix on the left-hand side of (7.5) is invertible always (this follows from the fact that $\sigma_+(\lambda)$ is a simple eigenvalue), and so (7.5) can be formulated as a differential equation for $\zeta_+(\lambda)$ in the λ plane, and therefore it provides a framework for *numerical analytic continuation*. This numerical analytic continuation will not be needed in this paper, but it is needed if one wants to use Cauchy's theorem to find numerically the number of eigenvalues inside a specific contour.

7.3. The boundary conditions at the compliant wall on $\bigwedge^3(\mathbb{C}^6)$

The induced boundary condition at the wall on $\bigwedge^3(\mathbb{C}^6)$ is constructed as follows. We propose that the correct boundary condition is

$$\mathbf{a}_1(\lambda)\wedge\mathbf{a}_2(\lambda)\wedge\mathbf{a}_3(\lambda)\cdot\mathbf{U}(0,\lambda)=0, \tag{7.6}$$

where the vectors $\mathbf{a}_j(\lambda)$ are the boundary condition vectors in the compliant wall boundary conditions (6.4), and the $\cdot$ represents a real dot product on $\bigwedge^3(\mathbb{C}^6)$.

To verify this, we need to derive a representation for the inner product on $\bigwedge^3(\mathbb{C}^6)$. Consider the real case: the inner product on $\mathbb{R}^6$, denoted $\langle\cdot,\cdot\rangle$ induces an inner product on the vector space $\bigwedge^3(\mathbb{R}^6)$ as follows. Let

$$\mathbf{x}=\mathbf{x}_1\wedge\mathbf{x}_2\wedge\mathbf{x}_3\quad\text{and}\quad\mathbf{y}=\mathbf{y}_1\wedge\mathbf{y}_2\wedge\mathbf{y}_3$$

be any real decomposable 3-forms. Then the inner product of $\mathbf{x}$ and $\mathbf{y}$ is defined by

$$[\![\mathbf{x},\mathbf{y}]\!]_3=[\![\mathbf{x}_1\wedge\mathbf{x}_2\wedge\mathbf{x}_3,\mathbf{y}_1\wedge\mathbf{x}_2\wedge\mathbf{x}_3]\!]_3\stackrel{\text{def}}{=}\det\begin{bmatrix}\langle\mathbf{x}_1,\mathbf{y}_1\rangle & \langle\mathbf{x}_1,\mathbf{y}_2\rangle & \langle\mathbf{x}_1,\mathbf{y}_3\rangle\\ \langle\mathbf{x}_2,\mathbf{y}_1\rangle & \langle\mathbf{x}_2,\mathbf{y}_2\rangle & \langle\mathbf{x}_2,\mathbf{y}_3\rangle\\ \langle\mathbf{x}_3,\mathbf{y}_1\rangle & \langle\mathbf{x}_3,\mathbf{y}_2\rangle & \langle\mathbf{x}_3,\mathbf{y}_3\rangle\end{bmatrix}, \tag{7.7}$$

It is easy to check that this definition satisfies all the properties of an inner product.

Therefore given any decomposable element $\mathbf{U}\in\bigwedge^3(\mathbb{C}^6)$ the inner product

$$[\![\mathbf{a}_1\wedge\mathbf{a}_2\wedge\mathbf{a}_3,\mathbf{U}]\!]_3=0$$

only if the vectors that make up $\mathbf{U}$ satisfy the boundary conditions at $z=0$, leading to (7.6). The vector on the left-hand side of (7.6) can be expressed as an element $\bigwedge^3(\mathbb{C}^6)\cong\mathbb{C}^{20}$

$$\begin{aligned}\mathbf{q}(\lambda) &:= \mathbf{a}_1(\lambda)\wedge\mathbf{a}_2(\lambda)\wedge\mathbf{a}_3(\lambda)\\ &= \lambda(\cos\varepsilon-\sin\varepsilon)(0,q_2,q_3,0,0,0,0,q_8,0,0,0,0,0,q_{14},0,0,0,0,0,0),\end{aligned}\tag{7.8}$$

using the definitions of the $\mathbf{a}_j(\lambda)$ in (6.4) with

$$q_2=-\frac{(\cos\varepsilon+\sin\varepsilon)}{R_e\Gamma},\qquad q_3=-\frac{2(\cos\varepsilon+\sin\varepsilon)}{R_e\Gamma}-\frac{\gamma^2E_k}{R_e\Gamma}(\cos\varepsilon-\sin\varepsilon)+\mathrm{i}\gamma E_k^{3/2},$$
$$q_8=\frac{(\cos\varepsilon-\sin\varepsilon)}{R_e\Gamma},\qquad q_{14}=\frac{\mathrm{i}\lambda}{\gamma R_e\Gamma}.$$

Note that the hypothesis (6.5) appears in a clear way when the boundary conditions are applied on $\bigwedge^3(\mathbb{C}^6)$. Define the complex analytic function of λ,

$$D(\lambda)=\mathbf{q}(\lambda)\cdot\mathbf{U}(0,\lambda),\tag{7.9}$$

where $\mathbf{U}(0,\lambda)\in\bigwedge^3(\mathbb{C}^6)$ is the solution of (7.2) evaluated at $z=0$. The dot product is just the standard inner product on $\mathbb{R}^{20}$ (i.e., no complex conjugation). Therefore the boundary condition at $z=0$ is just $D(\lambda)=0$.

7.4. Eigenvalues and Newton's method

The stability problem reduces to finding zeros of the complex analytic function $D(\lambda)$. In this paper, the main tool we will use is Newton's method. For fixed values of the parameters, given a good first guess for λ, denoted by λ_0, a new sequence of approximations is given by

$$\lambda_{n+1}=\lambda_n-\frac{D(\lambda_n)}{D'(\lambda_n)},\quad n=0,1,\ldots.$$

Now, $D'(\lambda)=\mathbf{q}'(\lambda)\cdot\mathbf{U}(0,\lambda)+\mathbf{q}(\lambda)\cdot\frac{\partial}{\partial\lambda}\mathbf{U}(0,\lambda)$. The easy part of this construction is differentiating $\mathbf{q}(\lambda)$,

$$\mathbf{q}'(\lambda)=\frac{1}{\lambda}\mathbf{q}(\lambda)+\frac{\mathrm{i}\lambda}{\gamma R_e\Gamma}(\cos\varepsilon-\sin\varepsilon)\mathbf{e}_{14},$$

where $\mathbf{e}_{14}$ is the 20 dimensional vector with unity in the 14th entry and zero otherwise. To get an expression for $\partial_\lambda\mathbf{U}(0,\lambda)$, we integrate the augmented system

$$\frac{\mathrm{d}}{\mathrm{d}z}\begin{pmatrix}\mathbf{U}\\ \partial_\lambda\mathbf{U}\end{pmatrix}=\begin{bmatrix}\mathbf{A}^{(3)}(z,\lambda) & 0\\ \partial_\lambda\mathbf{A}^{(3)}(z,\lambda) & \mathbf{A}^{(3)}(z,\lambda)\end{bmatrix}\begin{pmatrix}\mathbf{U}\\ \partial_\lambda\mathbf{U}\end{pmatrix},\qquad\begin{pmatrix}\mathbf{U}(L_\infty,\lambda)\\ \mathbf{U}_\lambda(L_\infty,\lambda)\end{pmatrix}=\begin{pmatrix}\zeta_+(\lambda)\\ \zeta_+'(\lambda)\end{pmatrix},\tag{7.10}$$

where an explicit expression for the derivative of $\mathbf{A}^{(3)}(z,\lambda)$ is obtained by differentiating the original 6×6 matrix, $\mathbf{A}(z,\lambda)$, with respect to λ and then using the algorithm which takes the original matrix to the induced 20×20 matrix to find $\frac{\partial}{\partial\lambda}\mathbf{A}^{(3)}(z,\lambda)$, and $\partial_\lambda\zeta_+(\lambda)$ is obtained as shown in Section 7.2. Combining these constructions leads to a robust Newton algorithm to find roots of the complex function $D(\lambda)$.

8. Curves of neutral stability for the rigid wall

For the case of the Ekman boundary layer adjacent to a rigid wall, the parameter dependence of the linear stability problem reduces to four parameters: γ, ε, R_e and E_k. However it was noted at the end of Section 3 that E_k could be scaled out in this case, and hence we set $E_k=1$. The main goal of this section is to check the code and compare with existing results in the literature on the Ekman stability problem, by constructing neutral curves and the minimal Reynolds number.

In order to find a point on a curve of neutral stability, two of the parameters, e.g., γ and ε, are fixed at some reasonable values and the zeros of $\mathrm{Re}(\lambda)$ (equivalently $\mathrm{Im}(c)$) are found by varying the third parameter, R_e. Figs. 4 and 5 show two points of view of the neutral surface. Fig. 4 shows slices of constant R_e and Fig. 5 shows slices of constant ε.

In the computation of neutral curves a value of $L_\infty=10$ was used, and when computing the critical Reynolds number, the effect of L_∞ was checked and this data is shown in Table 2. The equations on $\bigwedge^3(\mathbb{C}^6)$ are integrated using a second-order Gauss–Legendre Runge–Kutta method. It was shown in [23] that GL-RK methods preserve quadratic invariants well, which is important when integrating on $\bigwedge^3(\mathbb{C}^6)$ (see comments in Section 11). Two types of numerical continuation were used in constructing the neutral curves. For simple curves, the continuation procedure used was just linear extrapolation, and this was used for constructing the curves in Fig. 5. The curves in Fig. 4 are more delicate and there an AUTO continuation procedure based on arc-length continuation was coupled with the equations.

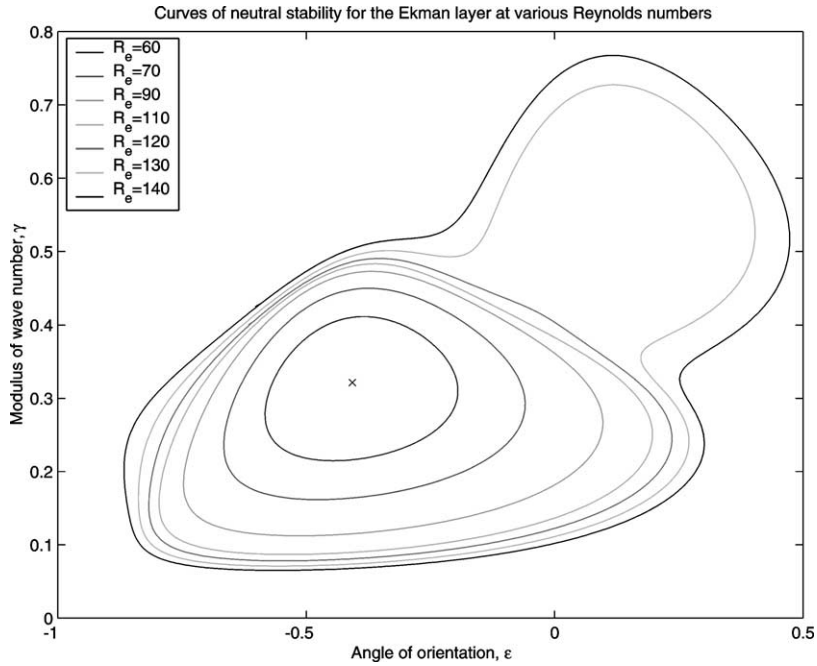

Fig. 4. Curves of neutral stability (constant R_e slices of the neutral surface) for the Ekman-layer for various Reynolds numbers in the (ε, γ) plane.

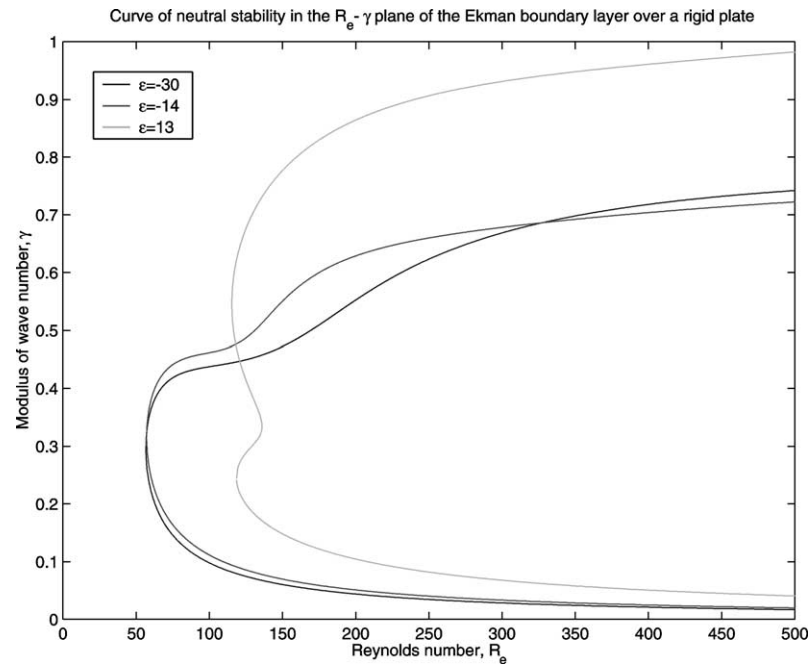

Fig. 5. Curves of neutral stability (constant ε slices of the neutral surface) for the Ekman layer in the (R_e, γ) plane for rotation angles: $-30°$, $-14°$ and $13°$.

The neutral curves in Fig. 4 show excellent agreement with existing results in the literature. The most accurate results to date are due to Melander [6] and Fig. 4 shows excellent qualitative agreement with Fig. 4(a) of [6]. A quantitative comparison

Table 1
Comparison of critical Reynolds number calculations for the Ekman layer with results in the literature

Reference	Wave type	R_e	αc_r	$2\pi/\alpha$	ε
Faller [15]	2	55	–	24	–15
	1	118	–	11	10–12
Lilly [4]	2	55	0.187	21	–20
	1	110	0.050	11.9	7.5
Iooss et al. [5]	2	54.2	0.195	19.88	–23.3
Melander [6]	2	54.15504	0.19489	19.869	–23.3261
	1	112.75847	0.05182	11.397	7.2021
Allen [27]	2	54.15504	0.19487	19.872	–23.3261

Table 2
Effect of stepsize and L_∞ on the critical Reynolds number

L_∞	Stepsize	Orientation angle, ε	Im(c)	Re(c)	Critical R_e
10	0.02	−23.3261087464691	−9.96864D–11	0.616278927369	54.1551938068
50	0.02	−23.3261087464691	−9.4532D–11	0.616072311672	54.1551889885
100	0.02	−23.3261087464691	8.0258D–11	0.616323500359	54.1550527485
500	0.02	−23.3261087464691	−7.21280D–11	0.616323500656	54.1550525485
300	0.01	−23.3261087464691	9.61736D–11	0.616323524212	54.1550413485
Melander	[6]	−23.32610874647	0	0.6163019690056	54.15503924999

is given in Table 1, and it is clear from this data that the numerical scheme shows excellent agreement with [6]. Table 2 then shows the effect of stepsize and L_∞ on the critical Reynolds number.

The neutral curve separates regions of linearly stable perturbations from linearly unstable regions. The Ekman spiral is unstable to perturbations corresponding to parameter values inside the contours. The critical Reynolds number of the class of perturbations is determined by minimisation of R_e under the constraint that $\mathrm{Re}(\lambda) = 0$. This point is marked by a $(\times)$ for the type-2 instability in Fig. 4 and is listed in Table 1 together with some existing theoretical results from the literature.

9. Numerical values for the compliant wall parameters

The compliant surface brings in a range of new parameters. The Ekman number can differ from one, and then there are the 5 dimensionless parameters (5.4) associated with the wall. The strategy is to use parameter values for the wall that have been used in the Blasius boundary layer interaction with a compliant surface [22]. Compliance has a noticeable effect on the neutral curves in the case of the Blasius boundary layer and so it provides a baseline to compare against.

In order to compare with the neutral curves in Section 8 the Ekman number will be set to unity. It was observed in [23] that wall damping and tension have little effect on the neutral curves (see however comments in the concluding remarks section). Therefore we consider only three nonzero parameters associated with the wall

$$C_m = \frac{\rho_m}{\rho}\frac{U_\infty b}{\nu}R_e^{-1}, \qquad C_B = \frac{BU_\infty}{\rho\nu^3}R_e^{-3}, \qquad C_{KE} = \frac{\nu k_E}{\rho u_\infty^3}R_e. \tag{9.1}$$

Parameter values of the physical quantities in these dimensionless numbers will be estimated using data that is typical of Kramer's experiments [22]. The fluid parameters are chosen to be representative of seawater

$$\rho = 1025\ \mathrm{kg}\cdot\mathrm{m}^{-3} \quad \text{and} \quad \nu = 1.37\times 10^{-6}\ \mathrm{m}^2/\mathrm{s}^{-1}.$$

The material density is chosen to be representative of natural rubber: $\rho_m = 945\ \mathrm{kg}\cdot\mathrm{m}^{-3}$, and the material thickness is taken to be $b = 2$ mm. The geostrophic velocity is taken to be $18\ \mathrm{m}\cdot\mathrm{s}^{-1}$. The material modulus B and spring function k_E are treated as functions of E, the wall rigidity,

$$B = 8.9\times 10^{-10}E\ \mathrm{N}\cdot\mathrm{m} \quad \text{and} \quad k_E = 230E,$$

where E is given in units of $\mathrm{N}\cdot\mathrm{m}^{-2}$. Substituting these values into (9.1) leads to the following expressions for the wall parameters

$$C_m = \frac{24226.421}{R_e},$$
$$C_B = 6078227.4\frac{E}{R_e^3}, \tag{9.2}$$
$$C_{KE} = 2.2918 \times 10^{-13}\,(230 E R_e).$$

Note that these coefficients are identical to those used for the Blasius interaction with a compliant surface (cf. [23] Eq. (7.4)). This correspondence was chosen, because if the Coriolis force is neglected, the linear stability equations (3.6) reduce to the Orr–Sommerfeld equation, and therefore the stability properties should be similar to those of the Blasius-wall interaction. However, we find that the Coriolis term leads to rather different behaviour.

10. Curves of neutral stability for the Ekman-compliant wall interaction

With the form for the coefficients (9.2) the wall is represented by a single parameter E, the wall rigidity, and $E \to \infty$ corresponds to the rigid wall. The stability problem now depends on four parameters: R_e, γ, ε and E. In this section we present some preliminary results on the effect of compliance. Choosing a representative neutral curve from Section 8 we compute the effect of varying E.

In Fig. 6, the computed effect of wall compliance on stability of the Ekman boundary layer flow is shown for the fixed Reynolds number $R_e = 60$. The parameter E is varied while keeping all other parameters fixed. The computed results show that wall compliance has an insignificant effect on the neutral curves at low Reynolds numbers, where the type-2 instability is dominant. Fig. 7 shows a blown-up version of Fig. 6 indicating that there is some quantitive effect although small. The only qualitative effect is that the trend is towards stabilization.

Although the results shown in the above figures are in strong contrast to the Blasius-wall interaction, where reducing E has a significant effect on neutral curves, they are consistent with the results of Cooper and Carpenter [18] for type-2 instabilities in the rotating disc. There they found that, in terms of neutral-stability curves, relatively low levels of wall compliance had a strong destabilizing effect on the type 2 instability, shifting the critical Reynolds number from a value well above that for the type 1 to a value well below (see Fig. 2 of [18]).

At larger Reynolds number, we also begin to observe a more noticeable effect on neutral curves. Fig. 8 shows the effect of wall compliance on the neutral curve for the Ekman boundary layer for fixed angle of orientation, $\varepsilon = -30.0$. The Reynolds number is allowed to vary to large values where the type-1 instability would begin to become dominant. There is a clear stabilization effect beginning to appear for the type-2 instability. The neutral curves for the Ekman compliant surface interaction

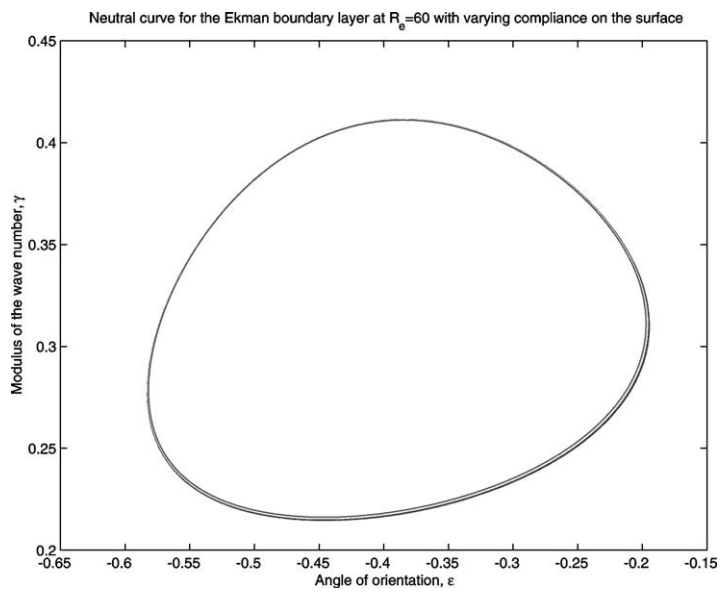

Fig. 6. Effect of wall compliance (represented by the wall rigidity E) for the Ekman layer at $R_e = 60$.

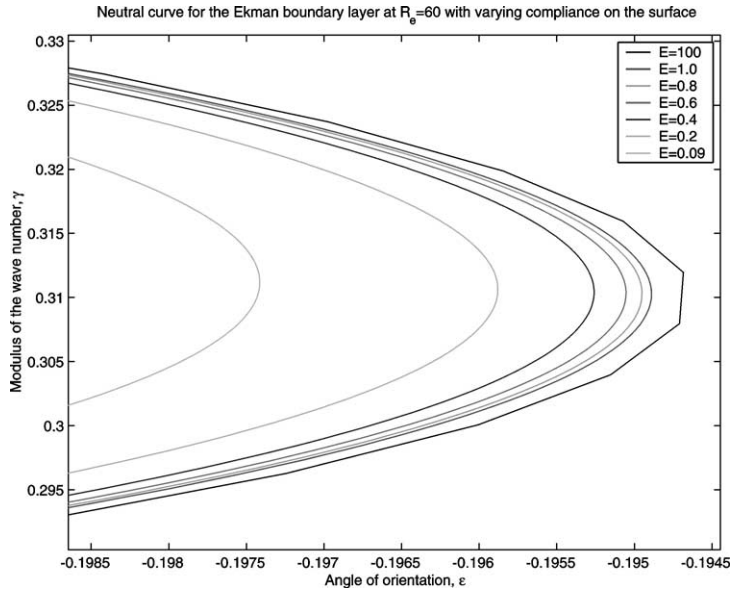

Fig. 7. Blow up of the neutral curve in Fig. 6 showing the small effect of wall compliance at $R_e = 60$.

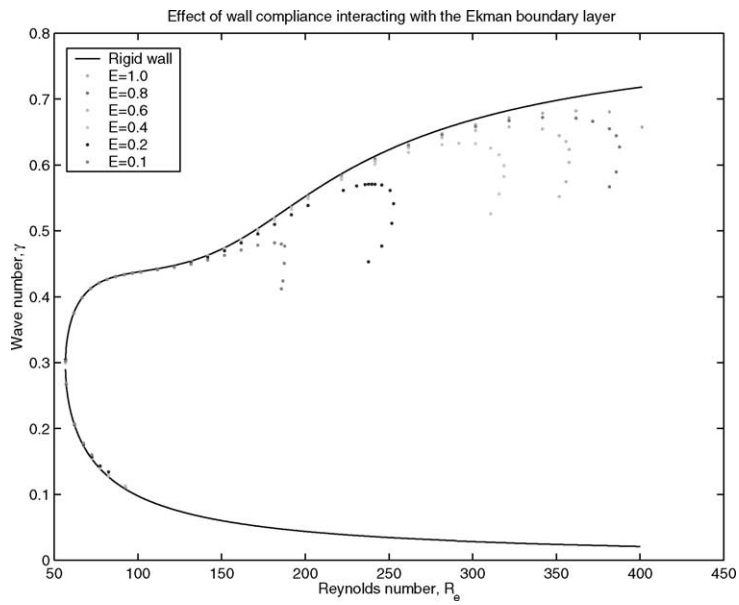

Fig. 8. Neutral curve for the Ekman layer for $\varepsilon = -30$ showing the effects of wall compliance.

begin to depart from the curve corresponding to the rigid wall by being displaced downwards and start to show a turning point similar to those observed in the Blasius-wall interaction [22,23].

The dotted curves in Fig. 8 end because a singularity is encountered, which we suspect is associated with a mode coalescence, since in the Newton scheme the derivative $D'(\lambda)$ tends toward zero at that point.

11. Concluding remarks

A model and numerical framework for the stability of the Ekman boundary layer, a three-dimensional rotating mean flow, have been presented. Our preliminary numerical results suggest that wall compliance has a very weak effect on the stability of Ekman-type rotating flows.

Of the possible choices of numerical method for the stability problem, such as matrix methods (finite difference, spectral methods), shooting with orthogonalization, shooting with compound matrices, we argued that a scheme based on the latter has the best features for stability problems of this type. Asymptotically exact boundary conditions can be used at $z = L_\infty$ in a way that preserves analyticity.

There is an open question about the numerical integration on $\bigwedge^3(\mathbb{C}^6)$ however. We argued for the use of Gauss–Legendre Runge–Kutta methods, and the numerical results certainly support this choice. However, a central feature of integration on $\bigwedge^3(\mathbb{C}^6)$ is the appearance of quadratic functions which should be preserved by the integrator. These functions define the Grassmannian, which is the manifold of three-dimensional subspaces, and it is implicit in the whole construction that this manifold be preserved. For the case of $\bigwedge^2(\mathbb{C}^4)$ there is only one quadratic function and it is proved in [23] that this invariant is preserved to machine accuracy when integrating the Orr–Sommerfeld equation on $\bigwedge^2(\mathbb{C}^4)$ using a GL-RK method. However, the preservation of the Grassmannian on $\bigwedge^3(\mathbb{C}^6)$ is still an open question.

The results presented here on interaction between the Ekman layer and a compliant surface suggest little impact of compliance on hydrodynamic stability. But it is clear that a wider parametric study is needed before definitive conclusions can be drawn. Some questions are: (a) what is the effect of compliance on the type-1 and type-3 Ekman instabilities? (b) While there is little effect on the neutral curve, what is the effect on the value of the growth rates for unstable waves? (c) Damping and tension have negligible effect in the Blasius wall interaction. However, there are cases where damping has been shown to have substantial effect (cf. Wiplier and Ehrenstein [32]. Will damping or tension have any effect in the rotating 3D case? (d) Will a different wall model have a different effect? (e) What is the effect of changing the Ekman number? (f) What is the singularity that is encountered in Fig. 8? (g) Is there a physical application of the Ekman compliant wall interaction?

Appendix

In this appendix, the explicit form for the induced matrix $\mathbf{A}^{(3)}(x,\lambda)$ is given, for the case where the standard basis for $\mathbb{C}^n$ is used. It is

$$
\begin{bmatrix}
1 & 2 & 3 & 4 & 5 & 6 & 7 \\
a11+a22+a33 & a34 & a35 & a36 & -a24 & -a25 & -a26 \\
a43 & a11+a22+a44 & a45 & a46 & a23 & 0 & 0 \\
a53 & a54 & a11+a22+a55 & a56 & 0 & a23 & 0 \\
a63 & a64 & a65 & a11+a22+a66 & 0 & 0 & a23 \\
-a42 & a32 & 0 & 0 & a11+a33+a44 & a45 & a46 \\
-a52 & 0 & a32 & 0 & a54 & a11+a33+a55 & a56 \\
-a62 & 0 & 0 & a32 & a64 & a65 & a11+a33+a66 \\
0 & -a52 & a42 & 0 & -a53 & a43 & 0 \\
0 & -a62 & 0 & a42 & -a63 & 0 & a43 \\
0 & 0 & -a62 & a52 & 0 & -a63 & a53 \\
a41 & -a31 & 0 & 0 & a21 & 0 & 0 \\
a51 & 0 & -a31 & 0 & 0 & a21 & 0 \\
a61 & 0 & 0 & -a31 & 0 & 0 & a21 \\
0 & a51 & -a41 & 0 & 0 & 0 & 0 \\
0 & a61 & 0 & -a41 & 0 & 0 & 0 \\
0 & 0 & a61 & -a51 & 0 & 0 & 0 \\
0 & 0 & 0 & 0 & a51 & -a41 & 0 \\
0 & 0 & 0 & 0 & a61 & 0 & -a41 \\
0 & 0 & 0 & 0 & 0 & a61 & -a51 \\
0 & 0 & 0 & 0 & 0 & 0 & 0
\end{bmatrix}
$$

$$
\begin{bmatrix}
8 & 9 & 10 & 11 & 12 & 13 & 14 \\
0 & 0 & 0 & a14 & a15 & a16 & 0 \\
-a25 & -a26 & 0 & -a13 & 0 & 0 & a15 \\
a24 & 0 & -a26 & 0 & -a13 & 0 & -a14 \\
0 & a24 & a25 & 0 & 0 & -a13 & 0 \\
-a35 & -a36 & 0 & a12 & 0 & 0 & 0 \\
a34 & 0 & -a36 & 0 & a12 & 0 & 0 \\
0 & a34 & a35 & 0 & 0 & a12 & 0 \\
a11+a44+a55 & a56 & -a46 & 0 & 0 & 0 & a12 \\
a65 & a11+a44+a66 & a45 & 0 & 0 & 0 & 0 \\
-a64 & a54 & a11+a55+a66 & 0 & 0 & 0 & 0 \\
0 & 0 & 0 & a22+a33+a44 & a45 & a46 & -a35 \\
0 & 0 & 0 & a54 & a22+a33+a55 & a56 & a34 \\
0 & 0 & 0 & a64 & a65 & a22+a33+a66 & 0 \\
a21 & 0 & 0 & -a53 & a43 & 0 & a22+a44+a55 \\
0 & a21 & 0 & -a63 & 0 & a43 & a65 \\
0 & 0 & a21 & 0 & -a63 & a53 & -a64 \\
a31 & 0 & 0 & a52 & -a42 & 0 & a32 \\
0 & a31 & 0 & a62 & 0 & -a42 & 0 \\
0 & 0 & a31 & 0 & a62 & -a52 & 0 \\
a61 & -a51 & a41 & 0 & 0 & 0 & a62
\end{bmatrix}
$$

$$
\begin{bmatrix}
15 & 16 & 17 & 18 & 19 & 20 \\
0 & 0 & 0 & 0 & 0 & 0 \\
a16 & 0 & 0 & 0 & 0 & 0 \\
0 & a16 & 0 & 0 & 0 & 0 \\
-a14 & -a15 & 0 & 0 & 0 & 0 \\
0 & 0 & a15 & a16 & 0 & 0 \\
0 & 0 & -a14 & 0 & a16 & 0 \\
0 & 0 & 0 & -a14 & -a15 & 0 \\
0 & 0 & a13 & 0 & 0 & a16 \\
a12 & 0 & 0 & a13 & 0 & -a15 \\
0 & a12 & 0 & 0 & a13 & a14 \\
-a36 & 0 & a25 & a26 & 0 & 0 \\
0 & -a36 & -a24 & 0 & a26 & 0 \\
a34 & a35 & 0 & -a24 & -a25 & 0 \\
a56 & -a46 & a23 & 0 & 0 & a26 \\
a22+a44+a66 & a45 & 0 & a23 & 0 & -a25 \\
a54 & a22+a55+a66 & 0 & 0 & a23 & a24 \\
0 & 0 & a33+a44+a55 & a56 & -a46 & a36 \\
a32 & 0 & a65 & a33+a44+a66 & a45 & -a35 \\
0 & a32 & -a64 & a54 & a33+a55+a66 & a34 \\
-a52 & a42 & a63 & -a53 & a43 & a44+a55+a66
\end{bmatrix},
$$

where aij represents the $a_{i,j}$th entry of the matrix $\mathbf{A}(z,\lambda)$. Note that this form agrees precisely with the form found by [33] using the compound matrix method. However, this form was obtained because *the standard basis for* $\mathbb{C}^6$ *was chosen*. If a different basis for $\mathbb{C}^6$ is chosen, then the resulting induced matrix would be different from that obtained with the compound matrix method.

References

[1] V.W. Ekman, On the influence of the earth's rotation on ocean currents, Ark. Math. Astronomi Fys. 2 (11) (1905) 53.
[2] J.P. Vanyo, Rotating Fluids in Engineering and Sciences, Butterworth–Heinemann, 1993.

[3] P.W. Carpenter, Status of transition delay using compliant walls, in: D.M. Bushnell, J.N. Hefner (Eds.), Viscous Drag Reduction in Boundary Layers, AIAA, 1990, pp. 79–113.
[4] D.K. Lilly, On the instability of Ekman boundary flow, J. Atmos. Sci. 23 (1966) 481–494.
[5] G. Iooss, H. Bruun, H. True, Bifurcation of the stationary Ekman flow into a stable periodic flow, Arch. Rat. Mech. Anal. 68 (1978) 227–256.
[6] M.V. Melander, An algorithmic approach to the linear stability of the Ekman layer, J. Fluid Mech. 132 (1983) 283–293.
[7] G.F. Spooner, Continuous temporal eigenvalue spectrum of an Ekman boundary layer, Phys. Fluids 25 (1982) 1958–1963.
[8] G.F. Spooner, W.O. Criminale, The evolution of disturbances in an Ekman boundary layer, J. Fluid Mech. 115 (1982) 327–346.
[9] I.H. Herron, Expansion problems in the linear stability of boundary layer flows, Adv. Appl. Math. 4 (1983) 260–297.
[10] P.R. Dwarka, I.H. Herron, The modulation equations for the asymptotic suction velocity profile and the Ekman boundary layer, Stud. Appl. Math. 96 (1996) 163–181.
[11] R.C. Foster, Structure and energetics of optimal Ekman layer perturbations, J. Fluid Mech. 333 (1997) 97–123.
[12] S.W. Marlatt, S. Biringen, On the spatial instability modes of the laminar Ekman boundary layer., J. Atmos. Sci. 51 (1994) 3539–3542.
[13] R.J. Lingwood, Absolute instability of the Ekman layer and related rotating flows, J. Fluid Mech. 331 (1997) 405–428.
[14] L. Greenberg, M. Marletta, The Ekman flow and related problems: spectral theory and numerical analysis, Math. Proc. Cambridge Phil. Soc., 2003, in press.
[15] A.J. Faller, An experimental study of the instability of the laminar Ekman boundary layer, J. Fluid Mech. 15 (1963) 560–576.
[16] A.J. Faller, R.E. Kaylor, A numerical study of the instability of laminar Ekman boundary layer flow, J. Atmos. Sci. 23 (1966) 466–480.
[17] R.J. Lingwood, Absolute instability of the boundary layer on a rotating disk, J. Fluid Mech. 299 (1995) 17–33.
[18] A.J. Cooper, P.W. Carpenter, The stability of rotating-disc boundary-layer flow over a compliant wall. Part 1. 1. Type I and II instabilities, J. Fluid Mech. 350 (1997) 231–259.
[19] C. Davies, P.W. Carpenter, Novel velocity–vorticity formulation of the Navier–Stokes equations for boundary-layer disturbances, Bull. Am. Phys. Soc. 40 (1995) 1956–1957.
[20] C. Davies, P.W. Carpenter, A novel velocity–vorticity formulation of the Navier–Stokes equations with applications to boundary-layer disturbance evolution., J. Comp. Phys. 172 (2001) 119–165.
[21] A.J. Cooper, P.W. Carpenter, The stability of rotating-disc boundary-layer flow over a compliant wall. Part 2. Absolute instability, J. Fluid Mech. 350 (1997) 261–270.
[22] P.W. Carpenter, A.D. Garrad, The hydrodynamic stability of flow over kramer-type compliant walls. Pt. 1: Tollmien–Schlichting Instabilities, J. Fluid Mech. 155 (1985) 465–510.
[23] L. Allen, T.J. Bridges, Numerical exterior algebra and the compound matrix method, Numer. Math. 92 (2002) 197–232.
[24] P.G. Drazin, W.H. Reid, Hydrodynamic Stability, Cambridge University Press, 1981.
[25] I.V. Barashenkov, E.V. Zemlyanaya, Oscillatory instabilities of gap solitons: a numerical study, Comput. Phys. Comm. 126 (2000) 22–27.
[26] T.J. Bridges, The Orr–Sommerfeld equation on a manifold, Proc. Roy. Soc. London Ser. A 455 (1999) 3019–3040.
[27] L. Allen, Modelling dolphin hydrodynamics: The numerical analysis and hydrodynamic stability of slow past compliant surfaces, Ph.D. Thesis, University of Surrey, 2002.
[28] W.A. Coppel, Stability and Asymptotic Behavior of Differential Equations, Heath, Boston, 1965.
[29] M.S.P. Eastham, The Asymptotic Solution of Linear Differential Systems: Applications of the Levinson Theorem, in: London Math. Soc. Monographs (N.S.), Oxford University Press, 1989.
[30] B.S. Ng, W.H. Reid, On the numerical solution of the Orr–Sommerfeld problem: Asymptotic initial conditions for shooting methods, J. Comput. Phys. 38 (1980) 275–293.
[31] T.J. Bridges, G. Derks, G. Gottwald, Stability and instability of solitary waves of the fifth-order KdV equation: a numerical framework, Physica D 172 (2002) 190–216.
[32] O. Wiplier, U. Ehrenstein, On the absolute instability in a boundary-layer flow with compliant coatings, Eur. J. Mech. B Fluids 20 (2001) 127–144.
[33] B.S. Ng, W.H. Reid, The compound matrix method for ordinary differential systems, J. Comput. Phys. 58 (1985) 209–228.